Advances in Geo-Energy Research

Vol. 2, No. 4, p. 380-392, 2018
www.astp-agr.com

Original article

Impacts of CO_2-brine-rock interaction on sealing efficiency of sand caprock: A case study of Shihezi formation in Ordos basin

Bin Liu[1,2], Xiaofei Fu[1]*, Zhuo Li[1]

[1]*Institute of Unconventional Oil-Gas, Northeast Petroleum University, Daqing 163318, P. R. China*

[2]*School of Electrical Engineering and Information, Northeast Petroleum University, Daqing 163318, P. R. China*

(Received July 14, 2018; revised August 2, 2018; accepted August 3, 2018; available online August 10, 2018)

Citation:
Liu, B., Fu, X., Li, Z. Impacts of CO_2-brine-rock interaction on sealing efficiency of sand caprock: A case study of Shihezi formation in Ordos basin. *Advances in Geo-Energy Research*, 2018, 2(4): 380-392, doi: 10.26804/ager.2018.04.03.

Corresponding author:
*E-mail: 760136897@qq.com

Keywords:
CO_2 geological storage
CO_2-brine-rock interaction
sand caprock
sealing efficiency

Abstract:
Large anthropogenic emission of CO_2 causes earth temperature becoming higher and higher, which may lead to the melting of glaciers, the rising of sea levels, extreme weather and so on. An effective way of reducing emissions is to capture and sequestrate CO_2 while not giving up the fossil fuels. Caprock seal is critical for CO_2 long term storage. CO_2-brine-rock interaction will change minerals composition and pore structure of both reservoir and caprock. This paper analyzes the variation trend of porosity and permeability due to CO_2-brine-rock interaction in caprock of Shihezi formation in Ordos basin, where TOUGHREACT is used as simulation tool. Geological data of numerical model are acquired from core samples. Simulations show that minerals interaction plays an important role on sealing efficiency of caprock. Overall, porosity and permeability of caprock decrease with CO_2 sequestration, which indicates that main mineral reaction in caprock is precipitation, and caprock sealing efficiency is enhanced.

1. Introduction

The emission of carbon dioxide released from burning coal is the main factor of climate change according to Intergovernmental Panel on Climate Change (IPCC) report (Metz et al., 2005; Busch et al., 2008). Chinese government has committed that CO_2 emission per unit of GDP by 2030 will be reduced to 60%∼65% over 2005 in United Nations Framework Convention on Climate Change. One of the effective ways to reduce CO_2 emissions is Carbon Capture and Sequestration (CCS). Caprocks, overlying gas and oil reservoirs, have the ability to prevent upward migration of hydrocarbons during geological time. In CO_2 geological storage, caprock sealing efficiency is also critical for CO_2 long term storage (Celia et al., 2005; Gaus, 2010; Kong et al., 2015). Since CO_2-brine-rock interactions last for a long time, minerals of caprock and its pore structure may be changed, which could alter the caprock sealing efficiency (Gaus et al., 2005; Xu et al., 2005).

Generally minerals dissolution and precipitation happen simultaneously during CO_2-brine-rock interaction (Chopping and Kaszuba, 2012; Galarza et al., 2013). If minerals dissolution is predominant, porosity and permeability will increase (Dong et al., 2012). Whereas if minerals precipitation predominates, porosity and permeability will decrease (Mitiku et al., 2013). Sometimes minerals dissolution may not weaken caprock sealing efficiency because of its dual function. On one hand, dissolution of carbonate minerals, such as calcite, will produce separation and partial migration of clay matrix between grains, which will cause porosity and permeability increase. On the other hand, clay particles enter pores and accumulate near the pore throat, which will not lead to porosity alteration but permeability decreasing dramatically (Yu et al., 2012). For example, clay mineral with expansive properties from chlorite and illite dissolution can reduce caprock porosity, which is beneficial to improve caprock sealing efficiency (Alemu et al., 2011). When minerals precipitation predominates during CO_2-brine-rock interaction, caprock sealing efficiency will be enhanced. In Sleipner project of Norway, dominant chemical reaction is carbonate precipitation. Although pH value is low, CO_2 accumulated under the caprock will

https://doi.org/10.26804/ager.2018.04.03.

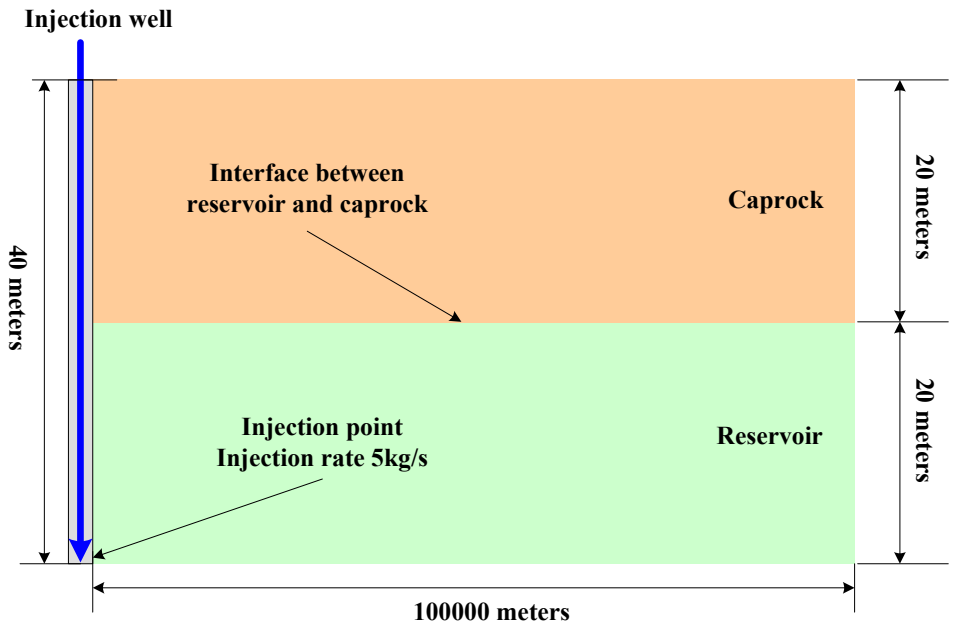

Fig. 1. Schematic of 2-D conceptual model.

facilitate cementation of carbonate minerals (Thomas, 2005). With pH value increasing, secondary minerals, such as pyrite cement produced by Belfast clay in Otway basin, are stacked in pore enhancing the caprock sealing efficiency significantly (Watson et al., 2005). Furthermore, the mineralization process of CO_2 in the form of ankerite and kaolinite will also improve caprock sealing efficiency (Watson et al., 2005).

CO_2-saline-rock interaction can be conducted in laboratory, where SEM, XRD are used to observe experimental phenomena and analyze results (Metz et al., 2005; Yu et al., 2012). Generally, geochemical reaction will last hundreds of years, even thousands of years. So, the experimental period is limited in laboratory (Credoz et al., 2011; Garrido et al., 2013; Olabode and Radonjic, 2013). Numerical simulation can reproduce multi-component solute transport process for thousands of years, where integrates several processes including fluid flow, solute transport and geochemical reaction (Gaus et al., 2005; Xu et al., 2005; Gaus, 2010; Dong et al., 2012; Yu et al., 2012; Mitiku et al., 2013).

Here TOUGHREACT V3.0-OMP and ECO2N module are used to analyze the variation trend of porosity and permeability of overlying caprock caused by CO_2-brine-rock interaction, by which flow, transport, and geochemical reaction equations are solved separately by means of a sequential iteration.

2. Research area

2.1 Background

Coal, oil and chemical industries have been developed in Ordos basin because of its richness in mineral resources, where CO_2 emission of coal to liquid project is up to 17.5 million tons (Zhai et al., 2016). The first CCS project in China was carried out in Ordos basin, whose injection is 0.1 million ton per year only. This is out of keeping with CO_2 emission of the region (Liu et al., 2015). Researches of CO_2-brine-rock interaction mostly focuses on storage capacity (Ming et al., 2015; Luo et al., 2016), injection ability analysis (He et al., 2016), reactions happening in reservoir, and so on (Xu et al., 2012; Li et al., 2016). CO_2 migration, distribution, and interaction after injection are of great significance for long safe sequestration, especially for how exerting influences on caprock sealing efficiency (Xu et al., 2006; Liu et al., 2014).

2.2 Numerical model

Geological data of numerical model are acquired from Shihezi formation in Ordos basin. The depth of storage site is 1860 meters, formation pressure 18.3 MPa, and temperature ranges between 55°C to 75°C. 2-D model is established to describe CO_2 migration process in both reservoir and caprock, as well as changes of both porosity and permeability because of minerals dissolution and precipitation due to CO_2-brine-rock interaction. The thickness of reservoir and caprock are 20 meters respectively, and the longitude distance is 10 km, which is depicted in Fig. 1. There are 20 layers in vertical aspect, each of which is 2 meters. CO_2 Injection well lies in the left side of 2-D model, and the injection point is in the left lower bottom. According to the impact of CO_2-brine-rock interaction, the sparse partitioning principle from left to right is adopted. The minimum grid is near the injection well. There are 16 grids from 0 to 100 meters, 20 grids from 100 to 1000 meters, 15 grids from 10000 to 100000 meters. There are 1120 grids in this 2-D model.

2.3 Parameters of numerical model

Both reservoir and caprock domains are modeled as porous media, parameters of which are detailed in Table 1. The

Table 1. Parameters of numerical model.

Parameter	Reservoir	Caprock
Thickness (meter)	20	20
Temprature (°C)	75	75
Pressure (MPa)	20	20
Density of rock (kg/m^3)	2600	2600
Porosity (%)	20	2.0
Horizontal permeability (m^2)	2.264×10^{-12}	2.264×10^{-17}
Vertical permeability (m^2)	2.264×10^{-13}	2.264×10^{-18}
Liquid relative permeability (Mualem, 1976; Van Genuchten, 1980)	$k_{rl}=\begin{cases}\sqrt{S^*}\left\{1-\left[1-(S^*)^{1/m}\right]^m\right\}^2 & S_l<S_{ls}\\ 1 & S_l\geq S_{ls}\end{cases}$ $S^*=\frac{(S_l-S_{lr})}{(1-S_{lr})}$	
Gas relative permeability (Corey, 1954)	$k_{rg}=\begin{cases}1-k_{rl} & S_{gr}=0\\ (1-\hat{S})^2(1-\hat{S}^2) & S_{gr}>0\end{cases}$ $\hat{S}=\frac{(S_l-S_{lr})}{(1-S_{lr}-S_{gr})}$	
Capillary pressure (Bear, 1972)	$P_c=-P_0\left[(S^*)^{-1/m}-1\right]^{1-m}$ $-P_{max}\leq P_c\leq 0$	

mineralogy of the model is described in terms of 8 primary minerals in reservoir, and 10 primary minerals in caprock, as shown in Table 2, where minerals volume fractions are listed. Full details on chemical composition of formation water can be referred (Wang et al., 2013), which is assumed to be representative of the fluids present in the reservoir and the caprock. Thermodynamic data for minerals, gases and aqueous species are mostly taken from the EQ3/6 V7.2b database.

In Table 1, m is fitting parameter, which is dependent on porosity, and is set to 0.457 in simulation; S_{lr} and S_{gr} are residual liquid-phase saturation, and residual gas-phase saturation; k_{rl} and k_{rg} are relative permeability of liquid and gas, respectively; S_l is liquid saturation; S_{ls} is saturation in liquid-saturated without capillarity, i.e., S_{ls} = 1 when capillary pressure is 0. Obviously, S^* and $\hat{S}$ are dimensionless saturation parameters. P_c is liquid capillary pressure, P_{max} is maximal capillary pressure, and P_0 is inlet pressure.

2.4 Kinetics of CO_2-brine-rock interaction

CO_2 will migrate towards to the interfacial of reservoir and caprock due to buoyancy after CO_2 injected into the reservoir, and enter into caprock under advection, diffusion, and pressure gradient. At the same time, CO_2 will dissolve into the formation water, which will promote various geochemical reactions. The acidification process can be described by following chemical equations (Gaus, 2010):

$$CO_{2(g)}+H_2O\rightarrow H_2CO_3 \quad (1)$$

$$H_2CO_3\rightarrow H^+ + HCO_3^- \quad (2)$$

Table 2. Minerals of reservoir and caprock (Wang et al., 2013).

NO.	Minerals	Reservoir (V%)	Caprock (V%)
1	Albite	12.500	25.000
2	Calcite	3.000	8.900
3	Illite	4.500	2.655
4	K-feldspar	4.500	4.600
5	Quartz	65.000	31.700
6	Smectite-Ca	1.250	0.116
7	Smectite-Na	1.250	0.116
8	Anorthite	8.000	24.700
9	Pyrite	—	1.400
10	Chlorite	—	0.813

$$HCO_3^-\rightarrow CO_3^{2-}+H^+ \quad (3)$$

With the decrease of pH value, dissolution and precipitation of minerals will occur in rock pore. When CO_2-brine-rock interaction including dissolution and precipitation of mineral reaches equivalent, the reaction rate equation is given by the following (Mitiku et al., 2013):

$$r_n=f(c_1,c_2,\ldots,c_{N_C})=\pm\alpha_n A_n\left|1-\Omega_n^{\theta}\right|^{\eta},\quad n=1,2,\cdots,N_q \quad (4)$$

Table 3. Parameters for kinetic rate law.

NO.	Mineral	Reactive surface area (m^2/g)	Neutral mechanism		Acid mechanism			Base mechanism		
			α_{25} (mol/m^2/s)	E_a (KJ/mol)	Weighting factor K_{25}	Activation energy	n(H^+) exponet	Weighting factor K_{25}	Activation energy	n(H^+) exponet
1	Albite	0.0483	9.52E-13	69.8	9.87E-11	65.0	0.457	2.512E-16	71.0	-0.572
2	Calcite	1.0E-3	1.55E-9	23.5	5.012E-04	14.4	1.000	1.55E-6	23.5	0.0
3	Illite	0.991	1.66E-13	35.0	1.047E-11	23.6	0.340	3.020E-17	58.9	-0.400
4	K-feldspar	0.0247	3.89E-13	38.0	8.710E-11	51.7	0.500	6.310E-22	94.1	-0.823
5	Quartz	0.0557	1.023E-14	87.7	-	-	-	-	-	-
6	Smectite-Ca	1.52E-2	1.7E-13	35.0	1.047E-11	23.6	0.340	3.020E-17	58.9	-0.400
7	Smectite-Na	1.52E-2	1.7E-13	35.0	1.047E-11	23.6	0.340	3.020E-17	58.9	-0.400
8	Anorthite	1.0E-3	7.6E-10	17.8	3.162E-04	16.6	1.411	2.75E-13	69.8	0.0
9	Pyrite	1.29E-3	-	-	3.02E-8	56.9	n(H^+)=-0.5 n(Fe^{3+})=0.5	2.8184E-5	56.9	n($O_{2(aq)}$)=0.5
10	Chlorite	2.0E-3	3.02E-13	88	7.762E-12	88.0	0.5	-	-	-
11	Magnesite	1.0E-3	4.57E-10	23.5	4.169E-7	14.4	0.5	-	-	-
12	Dawsonite	1.0E-3	1.26E-9	62.76	6.457E-06	36.1	0.5	-	-	-
13	Kaolinite	0.0987	6.61E-14	22.2	4.898E-12	65.9	0.777	8.913E-18	17.9	-0.472
14	Siderite	1.0E-3	1.66E-11	18.6	2.57E-9	18.6	0.28	-	-	-
15	Ankerite	1.0E-3	1.26E-9	62.76	6.46E-4	36.1	0.2	-	-	-

where positive values of r_n stand for dissolution, and negative values precipitation, A_n is the specific reactive surface area per kg H_2O (m^2/kg·w). Ω_n is the kinetic mineral saturation ratio defined by $\Omega_n = K_n^{-1}\prod_{j=1}^{N_C} C_j^{v_{nj}}\gamma_j^{v_{nj}}$, in which K_n is the corresponding equilibrium constant, $C_j^{v_{nj}}$ is mole concentration of the j-th basis species of n-th aqueous complex, $\gamma_j^{v_{nj}}$ is thermodynamic activity coefficient, θ and η are usually taken equal to 1. α_n is the rate constant, which is temperature dependent (Mitiku et al., 2013):

$$\alpha = \alpha_{25}\cdot\exp\left[\frac{E_a}{R}\left(\frac{1}{T}-\frac{1}{298.15}\right)\right] \tag{5}$$

where E_a is the activation energy (J/mol), α_{25} is the rate constant at 25°C (mol/m^2·s), R is gas constant (8.31 J/mol ·K), and T is absolute temperature (K).

The kinetic rate constant α_n and α in Eq. (4) and Eq. (5) only considers the most well-studied mechanism in pure H_2O at neural pH environment. Because of CO_2 injection, acid mechanism and base mechanism will catalyze dissolution and precipitation, and the kinetic rate constant α is expressed as (Mitiku et al., 2013):

$$\begin{aligned}\alpha = {} & \alpha_{25}^{nu}\cdot\exp\left[\frac{-E_a^{nu}}{R}\left(\frac{1}{T}-\frac{1}{298.15}\right)\right] \\ & + \alpha_{25}^{\mathrm{H}^+}\cdot\exp\left[\frac{-E_a^{\mathrm{H}^+}}{R}\left(\frac{1}{T}-\frac{1}{298.15}\right)\right]a_{\mathrm{H}^+}^{n_{\mathrm{H}^+}} \\ & + \alpha_{25}^{\mathrm{OH}^-}\cdot\exp\left[\frac{-E_a^{\mathrm{OH}^-}}{R}\left(\frac{1}{T}-\frac{1}{298.15}\right)\right]a_{\mathrm{OH}^-}^{n_{\mathrm{OH}^-}}\end{aligned} \tag{6}$$

where superscripts or subscripts nu, H^+ and OH^- indicate neutral, acid and base mechanism, respectively; $a_{\mathrm{H}^+}^{n_{\mathrm{H}^+}}$ and $a_{\mathrm{OH}^-}^{n_{\mathrm{OH}^-}}$ are the activities of H^+ and OH^-, respectively, which are calculated using the following expressions: $a_{\mathrm{H}^+}^{n_{\mathrm{H}^+}} = \gamma_{\mathrm{H}^+}c_{\mathrm{H}^+}$, $a_{\mathrm{OH}^-}^{n_{\mathrm{OH}^-}} = \gamma_{\mathrm{OH}^-}c_{\mathrm{OH}^-}$, where γ_{H^+} and γ_{OH^-} are thermodynamic activity coefficients of H^+ and OH^-, c_{H^+} and c_{OH^-} are mole concentration of H^+ and OH^-, respectively.

The changes in porosity with respect to mineral volume will be adopted to describe the evolution of sealing efficiency in caprock. Volume fraction will increase due to mineral precipitation, and decrease due to mineral dissolution during the mineralization of CO_2-brine-rock interaction. The change of porosity can be defined by (Xu et al., 2006):

$$\phi = 1 - \sum_{i=1}^{n_m} fr_i - fr_u \tag{7}$$

where ϕ is porosity, n_m is the total number of minerals, fr_i and fr_u are volume fractions of reactive minerals and nonreactive minerals in the rock.

Additionally, the relationship between absolute permeability and porosity has many expressions in different literature. The Carman-Kozeny equation can be used to compute the change of permeability with respect to porosity due to mineralization of CO_2-brine-rock interaction (Thomas et al., 2012):

$$\frac{kp}{kp_i} = \frac{(1-\phi_i)^2}{(1-\phi)^2}\cdot\left(\frac{\phi}{\phi_i}\right)^3 \tag{8}$$

where kp_i and ϕ_i are initial permeability and porosity, respectively; kp and ϕ are values after mineralization. This paper will analyze the change trend of rock porosity and permeability, and regard the porosity change as the index of sealing efficiency for caprock (Thomas et al., 2012).

From Eq. (4) - Eq. (6), kinetic rates are a product of rate constant and reactive surface area. Table 3 gives multiple

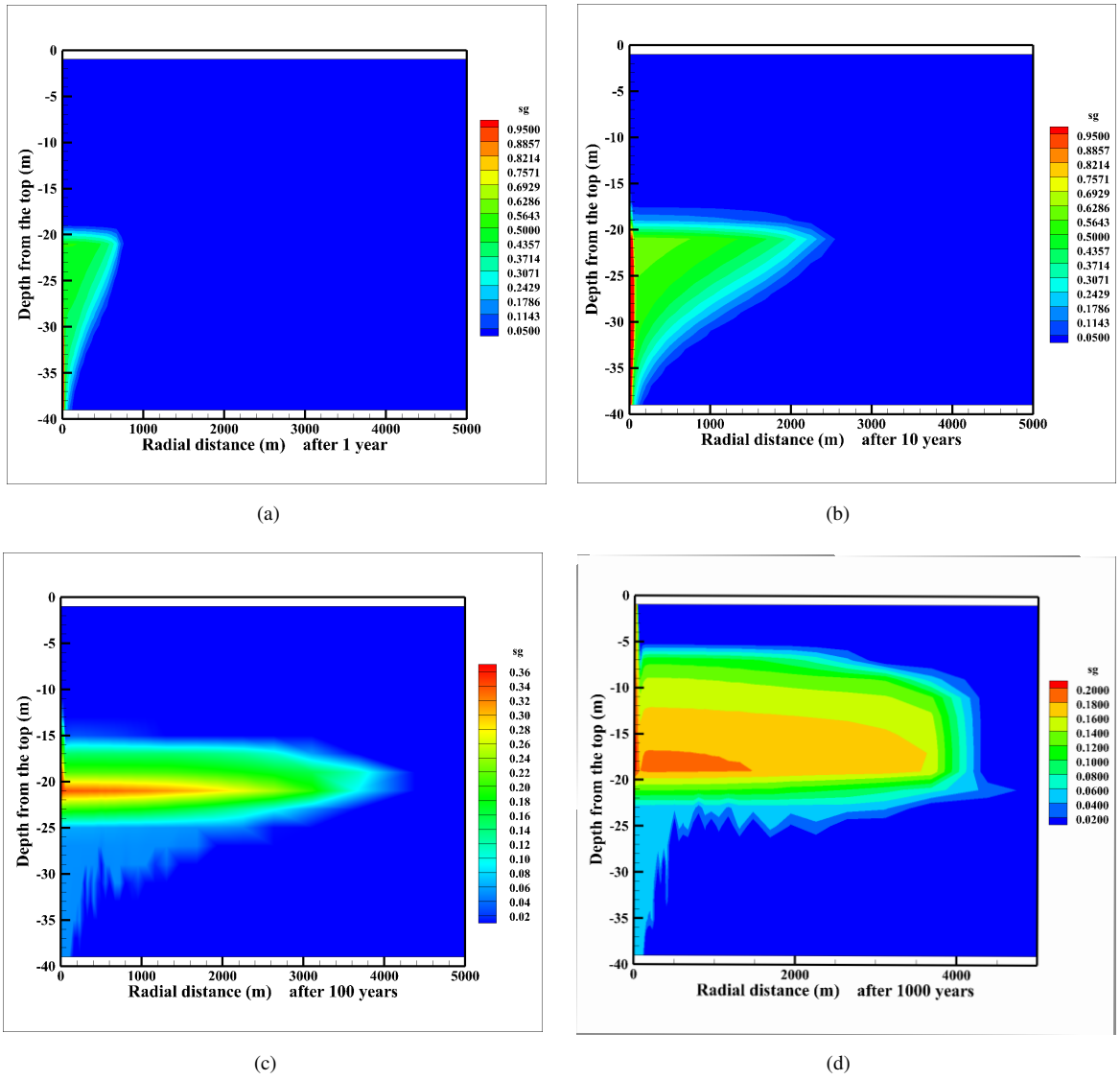

Fig. 2. Sg after CO_2 injection: (a). 1 year; (b). 10 years; (c). 100 years; (d). 1000 years.

mechanisms of minerals involved in numerical simulation, including neutral, acid and base mechanisms. Kinetic parameters are listed as: Reactive surface area, rate constant (α_{25}), the activation energy (E_a), the weighting factor K_{25}, and the power term (n) for each mechanism. These parameters are taken from TOUGHREACT V3.0-OMP reference manual (Xu et al., 2014).

3. Discussion of simulation results

Geochemical reactions play an important role in CO_2 geological storage environments, because they may change the properties of both reservoir and caprock. On one hand, primary minerals dissolution will promote CO_2 dissolution, some of which will be permanently trapped in the precipitating carbonates in a process referred to as mineral trapping in reservoir. On the other hand, minerals dissolution and precipitation may alter porosity and permeability of overlying lower caprock. Increasing with porosity and permeability, CO_2 leakage risk will become larger. Secondary minerals precipitation in caprock may decrease porosity and permeability of rock, which is beneficial to long sequestration.

Numerical simulations are conducted to model CO_2-brine-rock interaction in both reservoir and caprock of Shihezi formation in Ordos basin after CO_2 injection. The injection period is 1 year and long-term simulations are run to see changes about 1000 years.

3.1 Transport and distribution of gaseous CO_2

CO_2 will migrate upward with buoyancy after injection, some of which will move into both sides in horizontal because of the performance of caprock overlying the formation. Some CO_2 may enter the caprock under the pressure built up, diffusion, advection, or along rock fractures. Gas saturation (sg) is used to describe the distribution of gaseous CO_2 after injected into the formation, depicted in Fig. 2. During 10 years of after injection, a small amount CO_2 migrated into

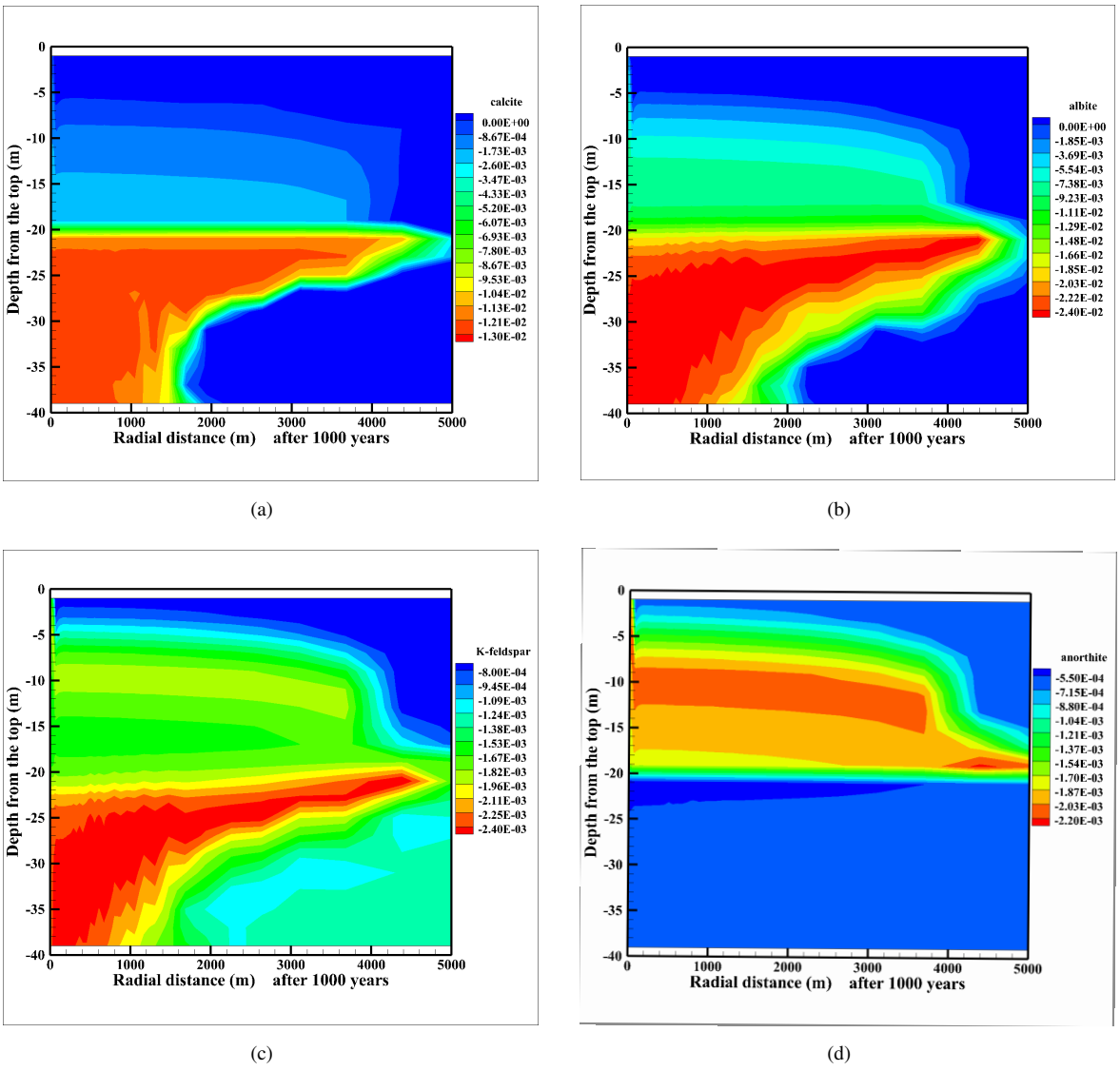

Fig. 3. Minerals dissolution after 1000 years simulation: (a). calcite; (b). albite; (c). K-feldspar; (d). anorthite.

the caprock, shown as Fig. 2(a) and Fig. 2(b). The horizontal distance will up to 4000 m when simulation is run 100 years, and the vertical distribution is symmetric with the interface between reservoir and caprock from Fig. 2(c). Gaseous CO_2 content is reduced immensely in reservoir after injection 1000 years depicted as Fig. 2(d). On the one hand, massive CO_2 is dissolved into the brine, which produces HCO_3^-, CO_3^{2-}, and H^+ by Eq. (1) - Eq. (3). On the other hand, the acidic environment promotes reactions in porous, and the reactions facilitate the CO_2 dissolution reversely. Little porosity and permeability of caprock limit the reaction rate and magnitude, which may be the main cause of large amounts of gaseous CO_2 existing in caprock.

3.2 Main reactions in CO_2 geological storage

According to Eq. (7), change of porosity is determined by minerals dissolution and precipitation. Some minerals volume fraction variations are illustrated in Fig. 3. In simulations, negative represents mineral dissolution while positive represents mineral precipitation. The largest change of calcite volume fraction is about 1.426%, albite 2.627%, K-feldspar 0.258%, and anorthite 0.226% after 1000 years simulation.

Calcite, illite and feldspar minerals dissolved largely with the strengthened of acidity, and corresponding chemical equations are described as following (Gaus, 2010):

Calcite dissolution:

$$\underbrace{CaCO_3}_{\text{calcite}} + H^+ \rightarrow Ca^{2+} + HCO_3^- \tag{9}$$

Illite dissolution:

$$\underbrace{K_{0.6}Mg_{0.25}Al_{2.3}Si_{3.5}O_{10}(OH)_2}_{\text{illite}} + 8\,H^+ \rightarrow 0.6K^+ + 0.25\,Mg^{2+} + 2.3\,Al^{3+} + 3.5\,SiO_{2(aq)} + 5\,H_2O \tag{10}$$

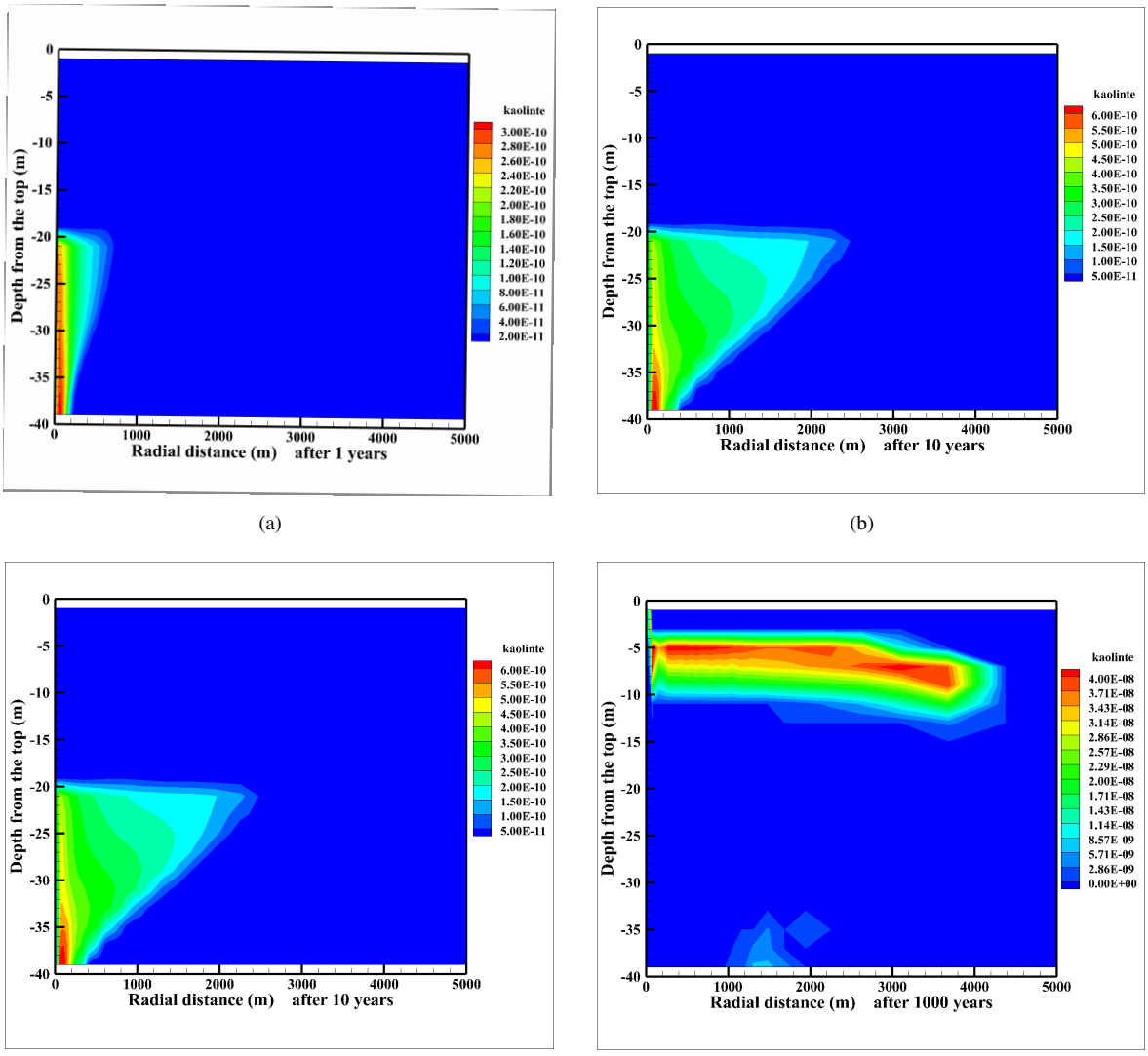

Fig. 4. Change of Kaolinite volume fraction: (a). 1 year; (b). 10 years; (c). 100 years; (d). 1000 years.

Albite dissolution:

$$\underbrace{NaAlSi_3O_8}_{\text{albite}} + 4\,H^+ \rightarrow Na^+ + Al^{3+} + 2\,H_2O + 3\,SiO_2 \quad (11)$$

K-feldspar dissolution:

$$\underbrace{KAlSi_3O_8}_{\text{K-feldspar}} + 4\,H^+ \rightarrow K^+ + Al^{3+} + 2\,H_2O + 3\,SiO_2 \quad (12)$$

Anorthite dissolution:

$$\underbrace{CaAl_2(SiO_4)_2}_{\text{anorthite}} + 8\,H^+ \rightarrow Ca^{2+} + 2\,Al^{3+} + 2\,SiO_2 + 4\,H_2O \quad (13)$$

Above minerals dissolutions provide a mass of cations: Ca^{2+}, Na^+, Al^{3+}, K^+, and Mg^{2+} in aqueous solution, which will provide reactive species when minerals precipitating, together with other cations included in formation water, Fe^{2+}, Cl^-, $SO_4{}^{2-}$, $NO_3{}^-$, and so on. Some of reactions are listed as following (Gaus, 2010):

$$\text{Feldspar} + H_2O + H^+ \rightarrow (K^+, Na^+, Ca^{2+}) + SiO_2 + \text{Kaolinite} \quad (14)$$

$$\text{Kaolinite} + K^+ \rightarrow \text{Illite} + H_2O + H^+ \quad (15)$$

Feldspar dissolution will lead to precipitations of kaolinite and dawsonite, where kaolinite is the product of feldspar and the reactant with K^+ for illite precipitation.

Changes of kaolinite volume fraction are described in Fig. 4, which is the main product of feldspar dissolution. After CO_2 injection 10 years, kaolinite is precipitated largely in reservoir, but almost none in caprock, illustrated in Fig. 4(a) and Fig. 4(b). In reservoir, kaolinite is precipitated mainly along front face in horizontal after 100 years, and there is less precipitation in the top of reservoir, shown in Fig. 4(c). From Fig. 4(d), it is found that kaolinite precipitation can be found in the middle of

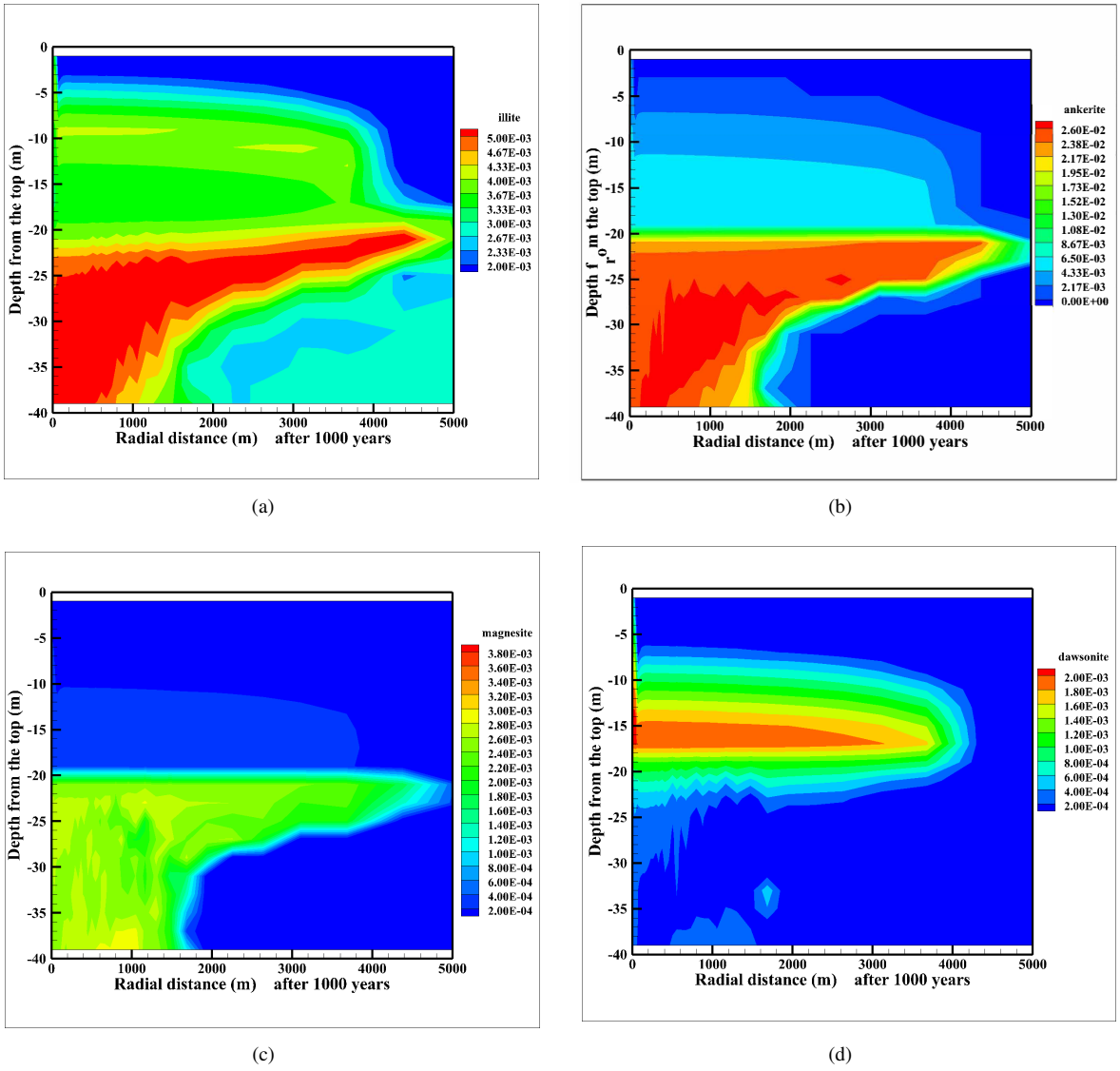

Fig. 5. Minerals precipitation after 1000 years simulation: (a). illite; (b). ankerite; (c). magnesite; (d). dawsonite.

caprock whereas scarcely any in reservoir in the last simulation period, which means that kaolinite precipitation has positive effect on promoting sealing efficiency of caprock.

After 1000 years simulation, illite, ankerite, magnesite and dawsonite precipitated in large amounts, and volume changes are 0.5456%, 2.716%, 0.395%, and 0.2103%, respectively. The contour plottings are portrayed in Fig. 5 and relevant reaction equations are listed as Eq. (15) - Eq. (18).

Ankerite precipitation:

$$Ca^{2+} + 0.3\,Mg^{2+} + 0.7\,Fe^{3+} + 4\,HCO_3^- \rightarrow \underbrace{CaMg_{0.3}Fe_{0.7}(CO_3)_2}_{\text{ankerite}} + 2\,H_2O + 2\,CO_2 \tag{16}$$

Magnesite precipitation:

$$Mg^{2+} + 2\,HCO_3^- \rightarrow \underbrace{MgCO_3}_{\text{magnesite}} + H_2O + CO_2 \tag{17}$$

Dawsonite precipitation:

$$Na^{+} + Al^{3+} + 4\,HCO_3^- \rightarrow \underbrace{NaAlCO_3(OH)_2}_{\text{dawsonite}} + H_2O + 3\,CO_2 \tag{18}$$

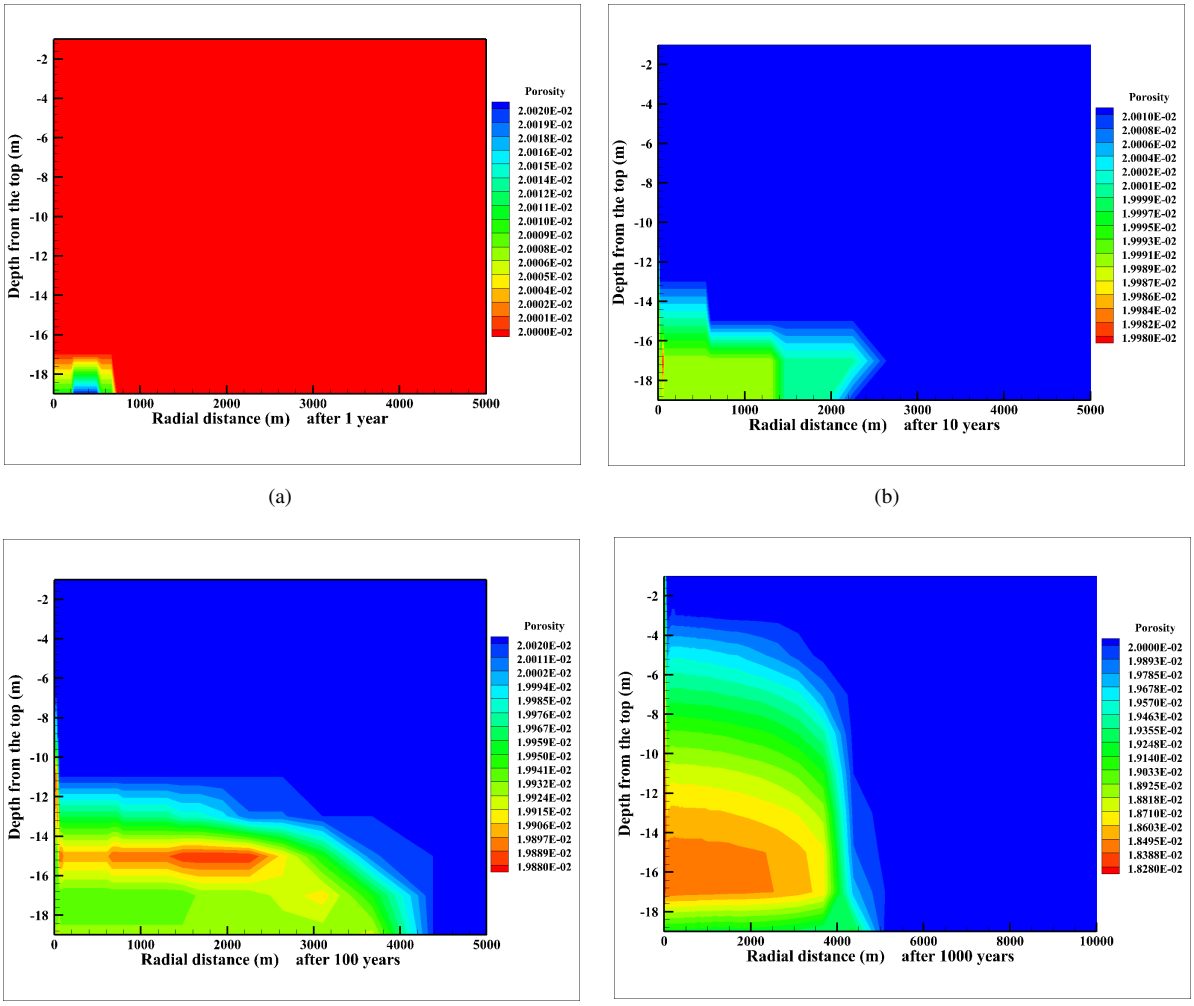

Fig. 6. Change of porosity in caprock: (a). 1 year; (b). 10 years; (c). 100 years; (d). 1000 years.

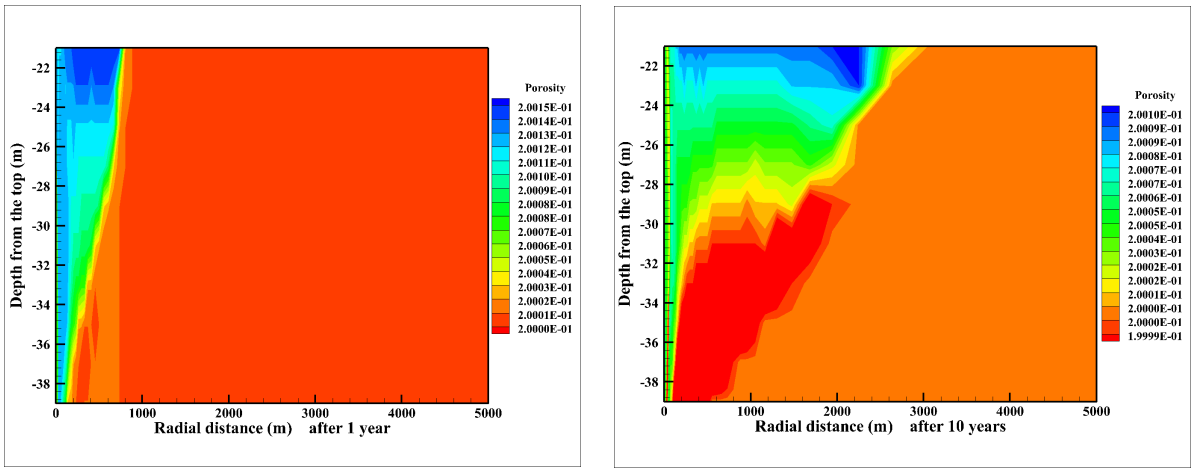

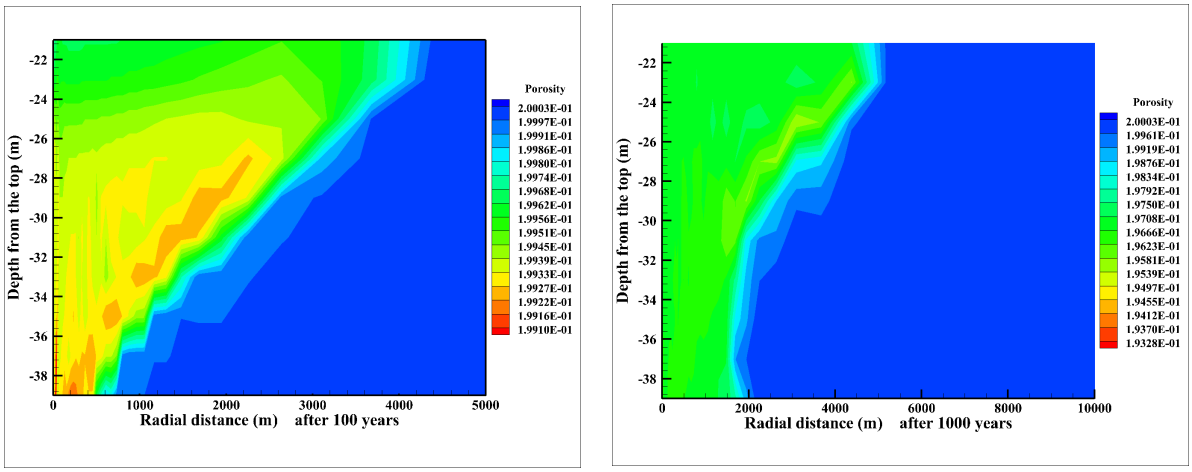

(c) (d)

Fig. 7. Change of porosity in reservoir: (a). 1 year; (b). 10 years; (c). 100 years; (d). 1000 years.

Albite precipitation is dependent of high CO_2 partial pressure at weakly alkaline environment (Qu et al., 2006). A mount of CO_2 is consumed with minerals in reactions so that pH value increases around the interface of reservoir and caprock, which coincide with dawsonite precipitation condition, as depicted in Fig. 5(d).

3.3 Evolution of sealing efficiency in caprock

Porosity will be adopted as the index of sealing efficiency of caprock. Porosity changes of reservoir and caprock are depicted in Fig. 6 and Fig. 7 after 1000 years simulation.

At the first stage, caprock porosity will be enlarged due to gas ingression into the caprock about 1 meter, which is agreed with reservoir porosity, as compared by Fig. 6(a) and Fig. 7(a). In this case, minerals dissolution rates are faster than precipitation. After 10 years, caprock porosity has been decreasing gradually, which indicates minerals precipitation will predominant in post-injection. The above processes can be seen from Fig. 6(b), Fig. 6(c) and Fig. 6(d). The vertical distance of CO_2 intrusion is about 5 m after 10 years of CO_2 injection, and 15 m after 1000 years, where porosity decreased. It should be noted that the greatest decrease did not happened in the interface between caprock and reservoir, whereas in the area 2∼3 m above on the interface, depicted in Fig. 6(d). There are two main reasons for this phenomenon. Firstly, pH value is lower aqueous solution in bottom than in central part of caprock because of more CO_2 dissolution in aqueous solution, which may cause minerals dissolution intensively. Secondly, minerals reactions in caprock bottom are affected by reactions in the top of reservoir. From the comparison between Fig. 5(d) and Fig. 6(d), we will find that dawsonite precipitation area is consistent with porosity decreasing area, from which we deduced that dawsonite precipitation was the key factor for porosity decreasing.

Variation tendency of reservoir porosity is increase first and then decrease, as shown in Fig. 7. The first 10 years reservoir porosity increased, listed in Fig. 7(a) and Fig. 7(b), although

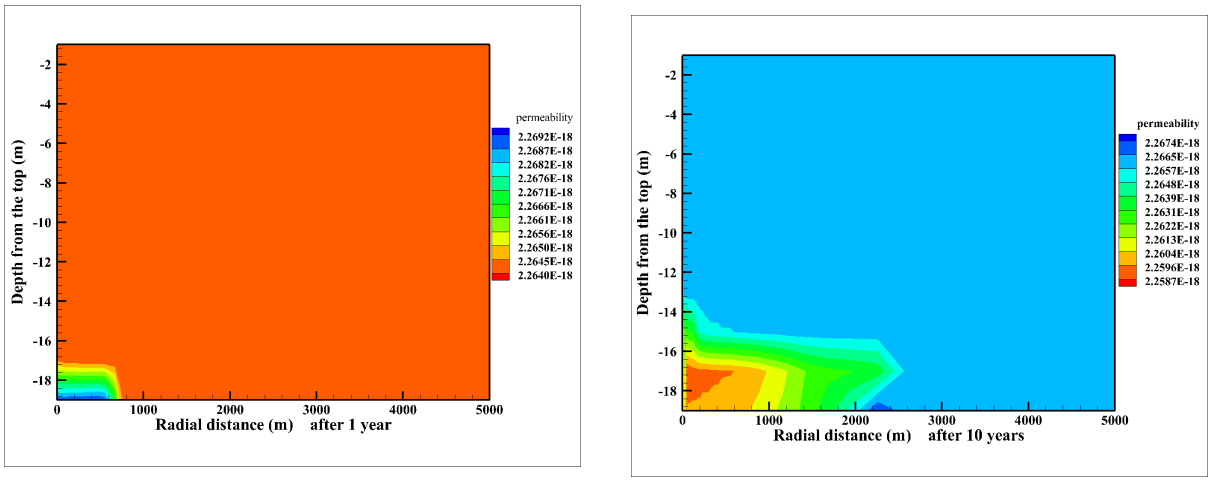

(a) (b)

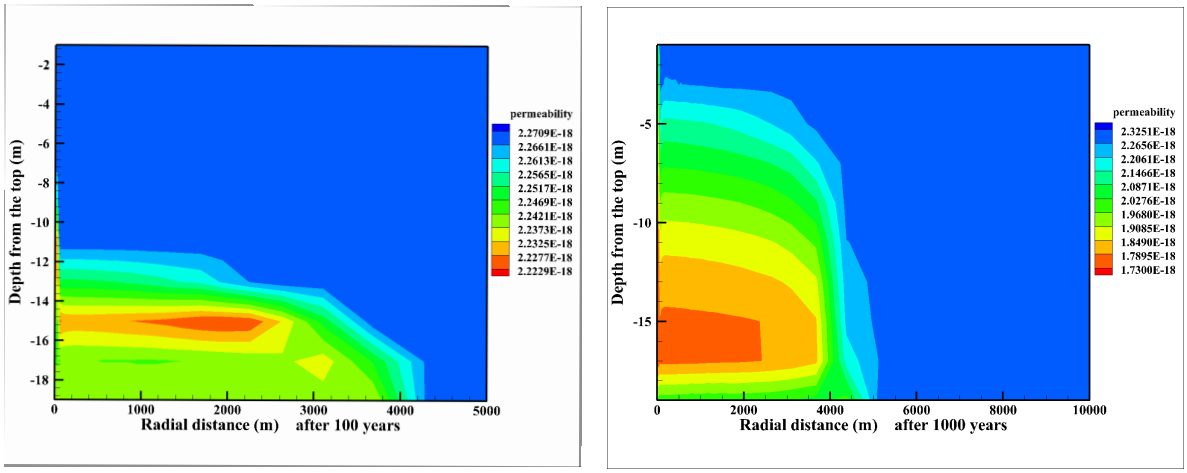

(c) (d)

Fig. 8. Change of permeability in caprock: (a). 1 year; (b). 10 years; (c). 100 years; (d). 1000 years.

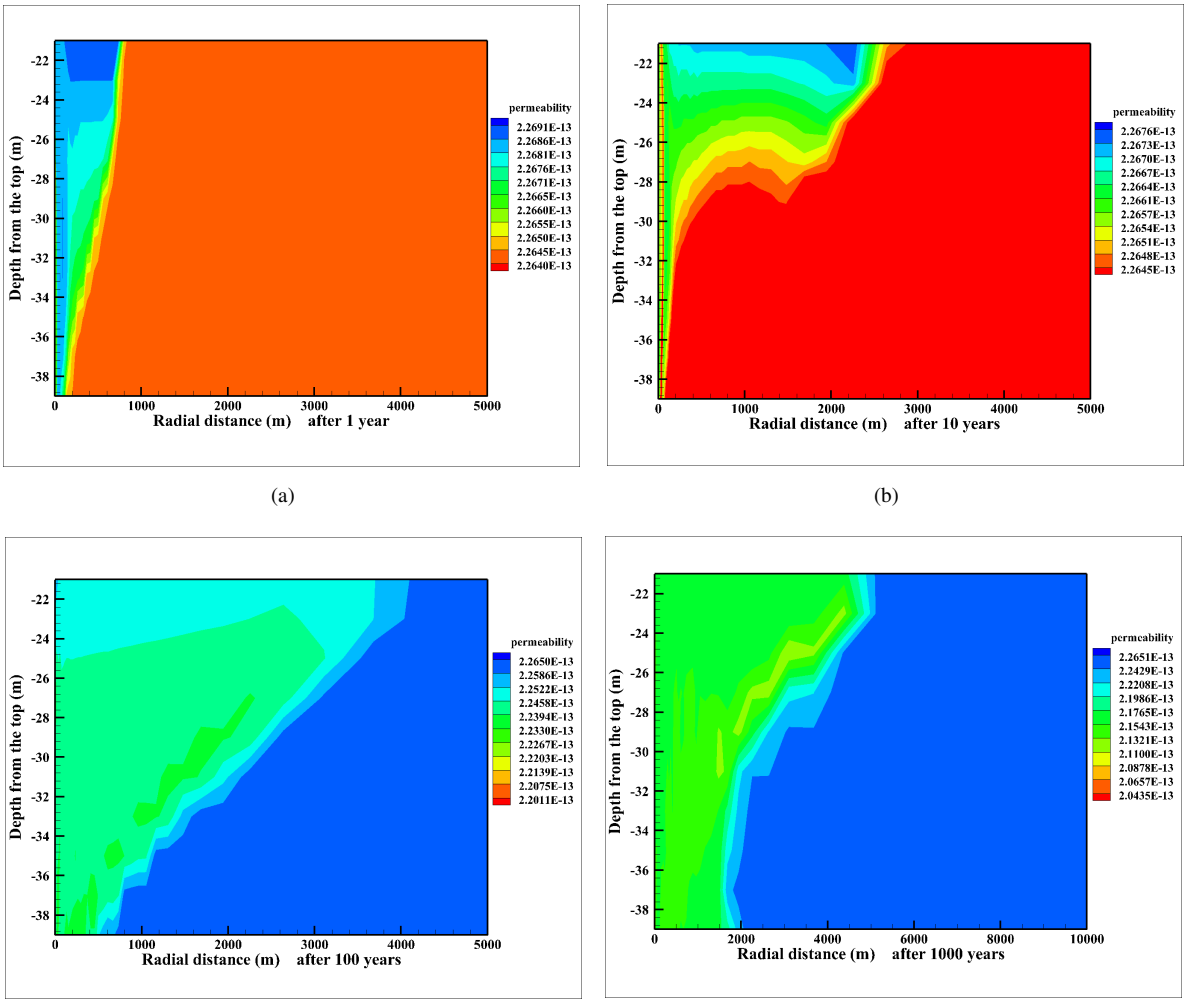

(a) (b)

(c) (d)

Fig. 9. Change of permeability in reservoir: (a). 1 year; (b). 10 years; (c). 100 years; (d). 1000 years.

Table 4. Changes percentage of both porosity and permeability in caprock and reservoir.

Year(s)	Caprock		Reservoir	
	Porosity (%)	Permeability (%)	Porosity (%)	Permeability (%)
1	0.0000	-4.4200	0.0600	0.1678
10	-0.0500	-0.1369	0.0200	0.0397
100	-0.3000	-0.9627	-0.2100	-0.6404
1000	-8.1000	-22.4210	-1.6150	-4.7783

the injection ended after 1-year injection. CO_2 gathered below the interface between caprock and reservoir because of buoyancy, which will result in low pH of aqueous solution. Mineral dissolutions play a dominant role because of abundant H^+. After 100 years injection, the main reason that leads to reservoir porosity decreasing is mineral precipitations, depicted in Fig. 7(c) and Fig. 7(d). In post-storage, precipitation is dominant, which is of great significance for CO_2 mineralization storage.

Permeability change of caprock and reservoir are illustrated in Fig. 8 and Fig. 9. From comparisons among Fig. 6, Fig. 7, Fig. 8 and Fig. 9, permeabilities of both caprock and reservoir agree with porosities of those, which increase firstly and then decrease.

Porosity and permeability of caprock will decrease with CO_2 sequestration, which indicate that main mineral reaction is precipitation. This implies that caprock sealing efficiency will be enhanced. To analyze changes of porosities and permeabilities of both reservoir and caprock quantitively, areas oriented below interface 2 m and above 2 m are chosen, whose horizontal distance are away from injection well. Changes percentage of both porosity and permeability in caprock and reservoir are listed in Table 4.

Relative variation ratio of porosity change in caprock is much greater than reservoir, and permeability is in the same way. This fact indicates that CO_2-brine-rock interactions affect caprock more than reservoir, which also demonstrates that minerals interaction plays an important role on sealing efficiency of caprock.

4. Conclusions

(1) CO_2-brine-rock interactions are enhanced in low pH environment, because of acidity in reservoir being strengthened due to CO_2 dissolution. In reservoir, calcite and feldspathoid are dissolved, and the volume fractions are decreased. Illite, ankerite, magnesite and dawsonite are precipitated, and the volume fractions are increased. On one hand, whether minerals are dissolved and precipitated, amount of CO_2 will be consumed, which will promote CO_2 dissolution in formation; on the other hand, CO_2-brine-rock interactions will result in CO_2 sequestrated underground. These processes may be very slow, but dissolved and mineralized deposits are ideal CO_2 storage.

(2) During CO_2 injection, the reservoir pressure is continuously increasing because of CO_2 injection. Large amount of CO_2 will enter into rock pore under the pressure, where the predominant CO_2-brine-rock interactions is minerals dissolution. Porosities of both reservoir and caprock will increase. It is beneficial to expanding storage capacity for reservoir, and the corresponding permeability will improve mobility of multiphase fluid. CO_2 migration will raise the efficiency of residual CO_2 storage and dissolved CO_2 storage. However, the caprock sealing efficiency will be weakened.

(3) A mass of CO_2 is accumulated below the interface of caprock and reservoir after CO_2 injection. At 10 years, the intrusion distance in caprock is 5 meters, and the caprock porosity becomes decrease since then. The longest distance into caprock is 15 m after CO_2 injection 1000 years, and the maximum of porosity change area is 5 meters above interface of caprock and reservoir, which is corresponding to the dawsonite precipitation area. Dawsonite precipitation has a positive significance for improving caprock sealing efficiency. In addition, the relative variation ratio of caprock porosity change is 8.1%, which is much larger than that of the reservoir 1.615%. This means that CO_2-brine-rock interactions have greater influence in porosity and permeability of caprock.

Acknowledgments

This work is supported by National Natural Science Foundation of China under Grant No. 41602134, U1562214, Project funded by China Postdoctoral Science Foundation under Grant No. 2017T100223, Natural Science Foundation of Heilongjiang Province under Grant No. D2017002.

References

Alemu, B., Aagaard, P., Munz, I., et al. Caprock interaction with CO_2: A laboratory study of reactivity of shale with supercritical CO_2 and brine. Appl. Geochem. 2011, 26(12): 1975-1989.

Bear, J. Dynamics of fluids in porous media. Eng. Geol. 1972, 7(2): 174-175.

Busch, A., Alles, S., Gensterblum, Y., et al. Carbon dioxide storage potential of shales. Int. J. Greenh. Gas Con. 2008, 2(3): 297-308.

Celia, M., Bachu, S., Nordbotten, J., et al. Quantitative estimation of CO_2 leakage from geological storage: Analytical models, numerical models, and data needs. Greenhouse Gas Control Technologies 2005, 1: 663-671.

Chopping, C., Kaszuba, J.P. Supercritical carbon dioxidebrine-rock reactions in the Madison Limestone of Southwest Wyoming: An experimental investigation of a sulfur-rich natural carbon dioxide reservoir. Chem. Geol. 2012, 322: 223-236.

Corey, A. The Interrelation between gas and oil relative permeabilities. Producers Monthly 1954, 19: 38-41.

Credoz, A., Bildstein, O., Jullien, M., et al. Mixed layer illite-smectite reactivity in acidified solutions: Implications for

clayey caprock stability in CO_2 geological storage. Appl. Clay Sci. 2011, 53(3): 402-408.

Dong, J., Li, Y., Yang, G., et al. Numerical simulation of CO_2-water-rock interaction impact on caprock permeability. Geological Science & Technology Information 2012, 31(1): 115-121.

Galarza, C., Buil, B., Peña, J., et al. Preliminary results from the experimental study of CO_2-brine-rock interactions at Elevated T & P: Implications for the pilot plant for CO_2 storage in Spain. Procedia Earth & Planetary Science 2013, 7: 272-275.

Garrido, D.R.R., Lafortune, S., Souli, H., et al. Impact of supercritical CO_2/water interaction on the caprock nanoporous structure. Procedia Earth & Planetary Science 2013, 7: 738-741.

Gaus I. Role and impact of CO_2-rock interactions during CO_2 storage in sedimentary rocks. Int. J. Greenh. Gas Con. 2010, 4(1): 73-89.

Gaus, I., Azaroual, M., Czernichowski-Lauriol, I. Reactive transport modelling of the impact of CO_2 injection on the clayey cap rock at Sleipner (North Sea). Chem. Geol. 2005, 217(3-4): 319-337.

He, B., Xu, T., Yuan, Y., et al. An analysis of the influence factors on CO_2 injection capacity in a deep saline formation: A case study of Shiqianfeng Group in the Erdos Basin. Hydrogeology & Engineering Geology 2016, 43(1): 136-142.

Kong, W., Bai, B., Li, X., et al. Sealing efficiency of combined caprock for CO_2 storage in saline aquifer. Chin. J. Rock Mech. Eng. 2015, 34: 2671-2678.

Li, F., Xu, T., Yang, L., et al. Numerical simulation for the water-rock interaction with the participation of CO_2 in different clastic mineral. Acta Petrolei Sinica 2016, 37(9): 1116-1128.

Liu, N., Liu, L., Ming, X., et al. Petrologic and geochemical characteristics and carbon sequestration capability of the Permian Shiqianfeng Formation around Ejin Horo Banner of Ordos Basin. Acta Petrologica Et Mineralogica 2014, 33(2): 255-262.

Liu, X., Wang, F., Yue, G., et al. Assessment of Sequestration Capacity of CO_2 in the Shihezi Formation, Ordos Basin. Bulletin of Mineralogy Petrology and Geochemistry 2015, 34(2): 395-400.

Luo, C., Jia, A., Wei, T., et al. CO_2 storage conditions and capacity in saline aquifer of Shan2 in Zizhou area, Ordos basin. Journal of Northeast Petroleum University 2016, 40(1): 14-24.

Metz, B., Davidson, O., De Coninck, H., et al. IPCC special report on carbon dioxide capture and storage. Cambridge University Press, 2005.

Ming, X., Liu, L., Liu, N., et al. Carbon sequestration potential of Yanchang formation sandstone of JX well, Ordos basin. Acta Sedimentologica Sinica 2015, 33(1): 202-210.

Mitiku, A., Li, D., Bauer, S., et al. Geochemical modelling of CO_2-water-rock interactions in a potential storage formation of the North German sedimentary basin. Appl. Geochem. 2013, 36(3): 168-186.

Mualem, Y. A new model for predicting the hydraulic conductivity of unsaturated porous media. Water Resour. Res. 1976, 12(3): 513-522.

Olabode, A., Radonjic, M. Experimental investigations of caprock integrity in CO_2 sequestration. Energy Procedia 2013, 37: 5014-5025.

Qu, X., Liu, L., Wang, Z., et al. Chemical features and origin of dawsonite-bearing stratum water in Wuerxun sag. J. Daqing Pet. Inst. 2006, 30(5): 7-10.

Thomas, D. Carbon dioxide capture for storage in deep geologic formations — Results from the CO_2 capture project. Amsterdam, Holand: Elsevier, 2005.

Thomas, M., Stewart, M., Trotz, M., et al. Geochemical modeling of CO_2 sequestration in deep, saline, dolomitic-limestone aquifers: Critical evaluation of thermodynamic sub-models. Chem. Geol. 2012, 306: 29-39.

Van Genuchten, M.T. A closed-form equation for predicting the hydraulic conductivity of unsaturated soils. Soil Sci. Soc. Am. J. 1980, 44: 892-898.

Wang, T., Wang, H., Zhang, F., et al. Simulation of CO_2-water-rock interactions on geologic CO_2 sequestration under geological conditions of China. Mar. Pollut. Bull. 2013,76(1-2): 307-314.

Watson, M., Daniel, R., Tingate, P., et al. CO_2-related seal capacity enhancement in mudstones: Evidence from the pine lodge natural CO_2 accumulation, Otway Basin, Australia. Greenhouse Gas Control Technologies 2005, 2(2): 2313-2316.

Xu, T., Apps, J., Pruess, K. Mineral sequestration of carbon dioxide in a sandstone-shale system. Chem. Geol. 2005, 217(3-4): 295-318.

Xu, T., Sonnenthal, E., Spycher, N., et al. Toughreact: A simulation program for non-isothermal multiphase reactive geochemical transport in variably saturated geologic media: Applications to geothermal injectivity and CO_2 geological sequestration. Comput. Geosci. 2006, 32(2): 145-165.

Xu, T., Sonnenthal, E., Spycher, N., et al. Toughreact V3.0-OMP sample problems. Lawrence Berkeley National Laboratory-Earth & Environmental Sciences, 2014.

Xu, Y., Zhang, K., Wang, Y. Numerical investigation for enhancing injectivity of CO_2 storage in saline aquifers. Rock & Soil Mechanics 2012, 33(12): 3825-3832.

Yu, Z., Liu, L., Yang, S., et al. An experimental study of CO_2-brine-rock interaction at in situ pressure-temperature reservoir conditions. Chem. Geol. 2012, 326-327(11): 88-101.

Zhai, M., Lin, Q., Zhong, L., et al. Economic assessment of carbon capture and storage combined with utilization of deep saline water. Modern Chemical Industry 2016, 36(4): 8-12.